ACS Energy LETTERS

Cite This: ACS Energy Lett. 2019, 4, 63−74

http://pubs.acs.org/journal/aelccp

LETTER

Rationalizing and Controlling the Surface Structure and Electronic Passivation of Cesium Lead Halide Nanocrystals

Maryna I. Bodnarchuk,[†] Simon C. Boehme,[§] Stephanie ten Brinck,[§] Caterina Bernasconi,[†,‡] Yevhen Shynkarenko,[†,‡] Franziska Krieg,[†,‡] Roland Widmer,[†] Beat Aeschlimann,[‡] Detlef Günther,[‡] Maksym V. Kovalenko,*[,†,‡] and Ivan Infante*[,§]

[†]Empa − Swiss Federal Laboratories for Materials Science and Technology, Überlandstrasse 129, CH-8600 Dübendorf, Switzerland

[‡]Institute of Inorganic Chemistry, Department of Chemistry and Applied Bioscience, ETH Zürich, Vladimir Prelog Weg 1, CH-8093 Zürich, Switzerland

[§]Department of Theoretical Chemistry, Faculty of Science, Vrije Universiteit Amsterdam, de Boelelaan 1083, 1081 HV Amsterdam, The Netherlands

Supporting Information

ABSTRACT: **Colloidal lead halide perovskite nanocrystals (NCs) have recently emerged as versatile photonic sources. Their processing and luminescent properties are challenged by the lability of their surfaces, i.e., the interface of the NC core and the ligand shell. On the example of $CsPbBr_3$ NCs, we model the nanocrystal surface structure and its effect on the emergence of trap states using density functional theory. We rationalize the typical observation of a degraded luminescence upon aging or the luminescence recovery upon postsynthesis surface treatments. The conclusions are corroborated by the elemental analysis. We then propose a strategy for healing the surface trap states and for improving the colloidal stability by the combined treatment with didodecyldimethylammonium bromide and lead bromide and validate this approach experimentally. This simple procedure results in robust colloids, which are highly pure and exhibit high photoluminescence quantum yields of up to 95−98%, retained even after three to four rounds of washing.**

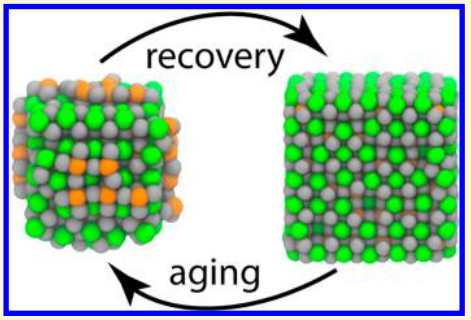

Surfaces have always been paramount to the electronic and photophysical quality and hence practical utility of semiconductors. This is particularly true for nanoscale semiconductors such as colloidal semiconductor nanocrystals (NCs) with inherently high surface-to-volume ratios.[1−3] Conventional semiconductor NCs, such as CdSe and InP, need to be overcoated with epitaxial shells (typically ZnS) for eliminating the localized surface states that act as traps for photogenerated electrons and holes, thus diminishing the photoluminescence quantum yields (PL QYs). Newcomers among highly luminescent semiconductor NCs (colloidal NCs of lead halide perovskites [$APbX_3$ NCs, A = Cs, formamidinium; X = Cl, Br, I, and mixtures thereof][4−8]) generally offer a much reduced density of surface trap states and greater tolerance of them.[9] The past few years have seen a surge of reports on these NCs, ranging from their synthesis,[4,10−18] structural and surface chemistries,[19−29] and doping[30−35] to optoelectronic applications such as in television displays,[36] light-emitting diodes,[37−43] or solar cells.[24,44,45] The compelling set of optical characteristics of $APbX_3$ NCs includes high absorption cross sections, high PL QYs (up to 100%), broadly tunable PL maxima (400−800 nm) with small PL full-width at half-maxima (fwhm, 12−50 nm for blue-to-near-infrared), and low thresholds for stimulated emission.[46,47] In addition, these NCs hold great promise as wavelength-tunable and controllable single-photon sources (with blinking-free single-photon emission, low spectral diffusion, ultranarrow line width of a few hundred microelectronvolts), capable of ultrafast emission (radiative lifetimes down to 100 ps at low temperature).[48−54] An Achilles' heel of all lead halide perovskite NCs is their inherent structural lability (low melting point, finite solubility in solvents, etc.), culminating at the NC surface. Highly dynamic binding exists between the surface capping ligands, typically a pair consisting of an anion (halide or oleate) and a cation (CS or alkylammonium), and the oppositely charged NC surface ions.[10,19,55,56] The ligand shell rapidly desorbs upon isolation and purification of colloids, causing the loss of

Received: September 6, 2018
Accepted: November 27, 2018
Published: November 27, 2018

DOI: 10.1021/acsenergylett.8b01669
ACS Energy Lett. 2019, 4, 63−74

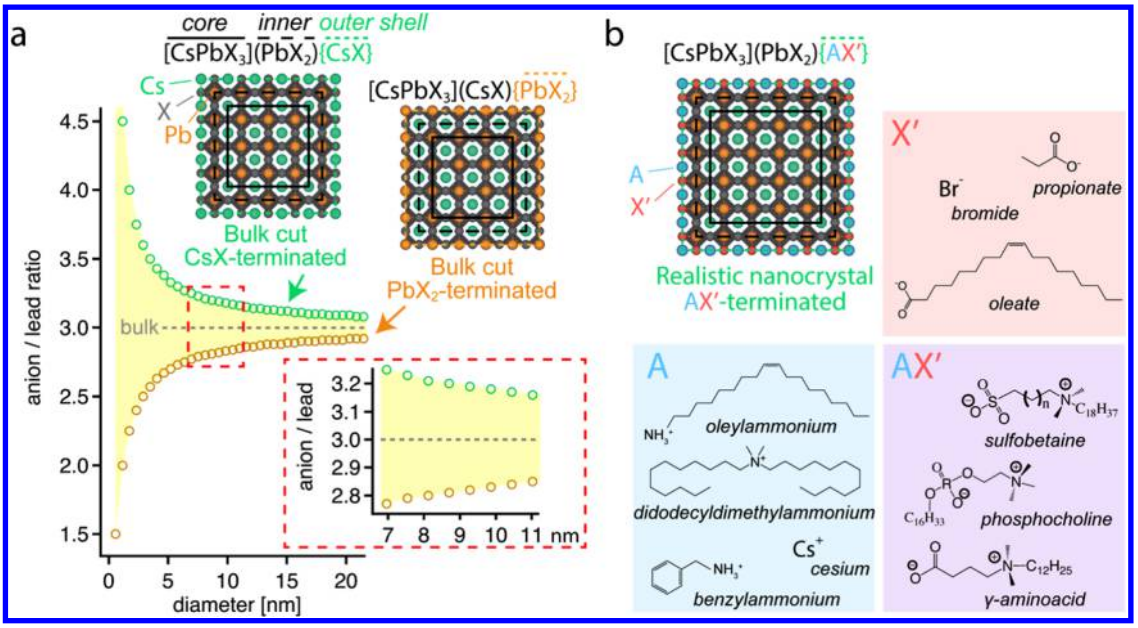

Figure 1. (a) Size-dependent anion/lead ratio (X/Pb) of cubic $CsPbX_3$ NCs, where Cs, Pb, and X (=halide) atoms are depicted by green, orange, and gray spheres, respectively. Unlike in the bulk, in a NC the anion/lead ratio deviates from three, with the upper bound (green circles) and lower bound (orange circles) given by CsX and PbX_2 termination, respectively. The inset shows commonly found experimental sizes, for which the anion/lead ratio should vary only between about 2.8 and 3.2, indicated by the yellow shaded area. (b) As explained in the main text, and to aid the discussion of aging, the NC is further (arbitrarily) divided into core, inner, and outer shell. For a realistic NC requiring colloidal stability, the outermost layer[61] is commonly replaced either by ligand pairs {AX′}, where A = cationic ligand (e.g., oleylammonium) and X′ = anionic ligand (e.g., bromide, oleate), respectively, or more recently also with zwitterionic ligands {AX′}, e.g., sulfobetaines. In either case, the anion/lead ratio (now [X + X′]/Pb) still falls within the yellow shaded area depicted in (a), and green circles correspond to full capping by the {AX′} ligand shell.

colloidal stability and eventually also the loss of structural integrity, i.e., the sintering of NCs into bulk polycrystalline materials. This surface damage then can extend beyond the ligand shell to the surface regions of the NCs, altering the surface stoichiometry and damaging the PbX_6 octahedra. Ultimately, the whole $CsPbX_3$ NC can alter its crystal structure, partially or fully converting to, for instance, CsX, $CsPb_2X_5$, PbX_2, or Cs_4PbX_6 phases,[57−65] or even fully disintegrate upon action of various solvents or complexing agents. Strategies for mitigating the instability issues include addition of new ligands or inorganic salts to the synthesis,[10,37,66−69] postsynthesis treatments of perovskite NCs,[22,23,25−27,47,70−72] and embedding of NCs into a solid matrix.[36,73−81]

In this study, we use density functional theory (DFT) to model the atomistic structure of the surfaces of $CsPbBr_3$ NCs for various degrees of the surface damage. We then compute the effect on the electronic structure and verify the eventual appearance of midgap trap states. On the basis of such a simple model, we rationalize the previously reported effects of the postsynthesis processing of perovskite NCs (ligand exchange, solvent effects, aging) on their luminescent characteristics (foremost PL QYs) and propose a general strategy for the elimination of the trap states by a simple surface treatment that invokes repair of surface PbX_6 octahedra and restoration of the ligand shell. Specifically, we show that the combined treatment with $PbBr_2$ and didodecylammonium bromide (DDAB) can recover the PL QY of the initially damaged NCs to values above 95%. This treatment also improves the colloidal durability of NCs, retaining their high PL QYs after three to four rounds of precipitation and redispersion. In addition, we discuss and demonstrate the utility and possible pitfalls of using the common techniques for elemental analysis, inductively coupled plasma-optical emission spectrometry (ICP-OES), and X-ray photoelectron spectroscopy (XPS).

Atomistic Structural Model of the $CsPbX_3$ Surface. An overarching goal of this study is to rationalize the inorganic surface of perovskite NCs, including its possible transformations under typical experimental conditions. We classify $CsPbX_3$ NCs and their surface termination by providing upper and lower bounds to their anion/lead (X/Pb) stoichiometry, a quantity that might be accessible experimentally (e.g., by XPS, ICP-OES, or ICP-mass spectrometry, Rutherford backscattering spectroscopy) and related to the quality of the surface (as evidenced, e.g., via PL QY measurements). In general, the upper bound for the anion/lead ratio is given by cutting a NC out of an orthorhombically distorted or, for simplicity, idealized cubic $CsPbX_3$ bulk lattice in such a way that Cs and X atoms form the outermost layer of the NC (see Figure 1a, open green circles and upper left schematic), denoted as $[CsPbX_3](PbX_2)\{CsX\}$. The lower X/Pb bound is given by cutting the NC such that it is terminated with a PbX_2 layer (orange open circles and lower schematic), named $[CsPbX_3]$-$(CsX)\{PbX_2\}$. The inset shows that in the commonly encountered size region of experiments, i.e., 7−12 nm, the halide/lead atomic ratio should only vary between about 2.7 and 3.3. We note that to obtain charge balance, i.e., a charge neutral NC with each element in its thermodynamically most favored oxidation state (+1 for Cs, +2 for Pb, −1 for X), a few surface cations need to be discarded for both the CsX-terminated and PbX_2-terminated cases. However, in Figure S1 we show that this leads only to a minor correction (<1%) for the anion/lead stoichiometric ratio in the experimental size region.

DOI: 10.1021/acsenergylett.8b01669
ACS Energy Lett. 2019, 4, 63−74

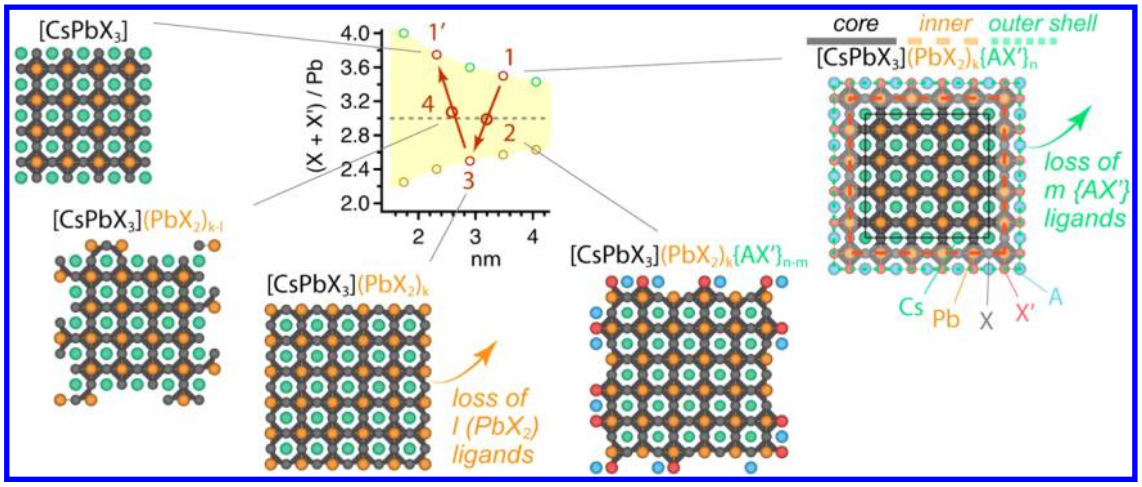

Figure 2. Plausible surface transformations illustrated for a 3.6 nm perovskite NC. The initial state "1" can be described as consisting of a $[CsPbX_3]$ core (continuous black line), surrounded by a shell of k (PbX_2) moieties (dashed orange line) and capped with n AX′-type ligands (dotted green line). To enhance clarity, the core is shown slightly smaller than in reality. Partial removal of m {AX′} units ($m < n$, state "2") or its complete elimination ($m = n$, state "3") leads to a (PbX_2)-terminated NC. Further detachment of l (PbX_2) units ($l < k$, state "4") eventually leads to a bare $[CsPbX_3]$ core ($l = k$, state "1", analogous to "1"). During the aging process, the anion/lead ratio oscillates from initially anion-rich (state "1") to Pb-rich (state "3") and back to anion-rich (state "1").

Realistic NCs are terminated with (long) insulating ligands, e.g., oleylammonium and oleate,[19,20] to render them colloidally stable by means of steric repulsion (Figure 1b). To account for ligand capping, we introduce a nomenclature in which we represent, e.g., the NC as $[CsPbX_3](PbX_2)\{AX'\}$ consisting of a $CsPbX_3$ core terminated by a PbX_2 (inner) shell and a capping AX′ (outer) shell, composed of monovalent cations (A = alkylammonium and Cs^+) and monovalent anions (X′ = halide and/or oleate). The proportion of the long-chain ions in the AX′ shell is governed by the steric hindrance and equilibria existing between the NC surface and solution. We note that our partition of the NC in core, inner, and outer shell regions is arbitrary, not intended to describe specific synthetic conditions, and solely intended to guide the rationalization of the experimental effects on the surface structure and optical properties.

The anion/lead ratio of an AX′-terminated NC is identical to that for the CsX-terminated case: a measurement of the anion/lead stoichiometry should yield the green data points in Figure 1a, if defined as (X + X′)/Pb, or the orange data points, if defined as X/Pb. In any case, it should vary only between about 2.8 and 3.2 for NCs of ∼10 nm. Alternatively, ligand capping can also be achieved by exposing PbX_2 termination, formed atop a CsX layer, i.e., as $[CsPbX_3](CsX)\{PbX'_2\}$. To achieve steric colloidal stabilization under typical synthesis conditions, X′ must be oleate. However, $\{PbX'_2\}$ termination is rather improbable as (i) it would require about 2.5 times denser ligand packing, leading to steric hindrance, and (ii) it breaks the propensity of Pb^{2+} to octahedral coordination. Furthermore, earlier studies[19] and our results discussed below point to the generic $[CsPbX_3](PbX_2)\{AX'\}$ structure as the most relevant to the known experimental facts about $CsPbX_3$ NCs.

Perovskite NC surfaces are fundamentally different from those of conventional semiconductor NCs in terms of their structural dynamics and lability. With perovskite NCs, an enormous degree of postsynthetic lability and reactivity has been reported and concerns the subsurface NC regions as well. Possible chemical reactions at the surfaces or involving the whole NCs may include mutual interconversion among $CsPbX_3$, CsX, $CsPb_2X_5$, and Cs_4PbX_6 phases under addition/subtraction of ligands and CsX and PbX_2 salts or other Cs, Pb, or X compounds.[57−65] These addition and elimination reactions are greatly influenced by the capping ligands and other reagents in the solution. Hence one can no longer assume the static picture of the rigid inorganic NC core coated with an organic shell. Surface and subsurface atoms are likely directly involved in all possible chemistry equilibria and transformations. A rather new mindset needs to be developed to rationalize the structure, reactivity, and electronic effects on an atomistic level.

Plausible Surface Transformations. Detachment of surface capping ligands is the most plausible surface transformation, for instance, as a result of environmental effects (moisture) or processing (repeated washing) and storage conditions. Figure 2 schematically depicts this process for a 3.6 nm NC, starting with the structure $[CsPbX_3](PbX_2)_k\{AX'\}_n$, where k and n are the numbers of (PbX_2) units and {AX′} ligands in the inner and outer shells, respectively. This idealized initial state "1" may now transform via removal of m {AX′} ligands (state "2"). A complete detachment of this ligand shell ($m = n$) yields a state "3", where a (PbX_2) layer is now fully exposed. Subsequent partial ($l < k$, state "4") or complete ($l = k$, state "1") removal of also the (PbX_2) shell exposes the bare $[CsPbX_3]$ core, which is effectively state "1", albeit with an overall reduction of NC diameter by one layer of octahedra. Figure 2 depicts the evolution of the anion/lead ratio (X + X′)/Pb throughout these surface processes, which varies initially from anion-rich to lead-rich and then back to anion-rich. This suggests that monitoring the anion/lead stoichiometry might give a hint to the possible surface structure/ligand capping. Indeed, our simplified model explains the XPS-derived postsynthetic transformations of both the outer {AX′} shell[15] and inner (PbX_2) shell.[22] We therefore propose that our simplified model presented in Figure 2 (which will further be refined in Figure 3c) may help to rationalize a broad range of experimentally observed surface transformation and guide the discussion of XPS-derived anion/lead stoichiometries.[15,22]

Electronic Structure at Various Surface Terminations. After having established plausible scenarios for the consecutive

DOI: 10.1021/acsenergylett.8b01669
ACS Energy Lett. 2019, 4, 63−74

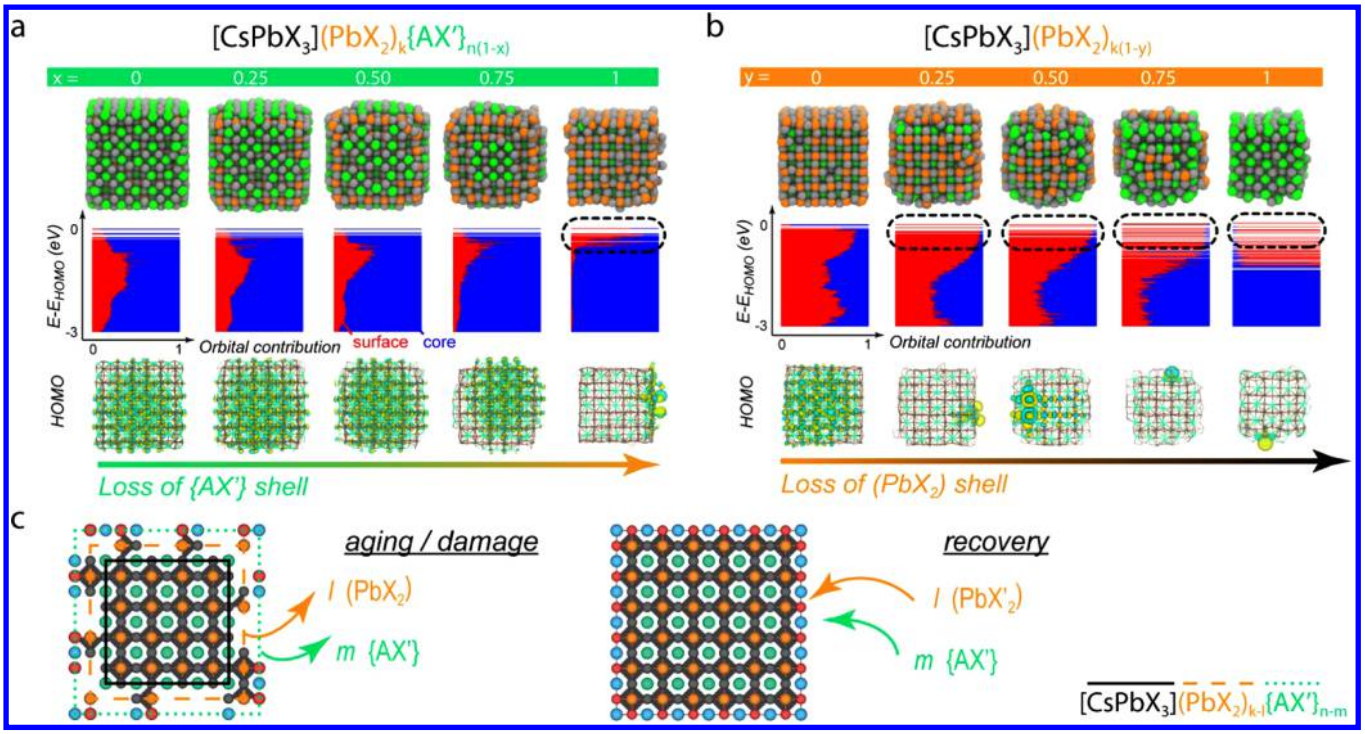

Figure 3. Computed geometry and electronic structure of $CsPbX_3$ NCs during the aging process introduced in Figure 2, at the DFT/PBE level of theory. (a) Loss of the outermost {AX′}-ligand shell of a $[CsPbX_3](PbX_2)_k\{AX'\}_{n(1-x)}$ NC, with X = X′ = Br, A = Cs, and $0 < x < 1$. The top row depicts the aging-induced changes to the geometry, where Pb, Cs, and Br atoms are depicted by orange, green, and gray spheres, respectively. The middle row shows the respective evolution of the valence band electronic structure from the HOMO ($E - E_{HOMO} = 0$) up to 3 eV below the HOMO, where relative orbital contributions by the core and surface (defined as the outermost, one-atom-thick layer) are depicted by blue and red bars, respectively. Surface-localized states only appear after loss of more than 75% of the {AX′} shell, indicated by a dashed ellipse and visualized in the bottom row via the associated localized valence band edge molecular orbitals (HOMOs). (b) Subsequent loss of the now exposed (PbX_2) shell. Localized states already appear at only 25% loss of the (PbX_2) shell. (c) Schematics of the aging/damage and recovery of trap-free $[CsPbX_3](PbX_2)_k\{AX'\}_n$ NCs.

removal of A, Pb, and X moieties from a NC, we calculate the corresponding geometries and electronic structures at the DFT level (see Supporting Information for further details). This allows us to judge if, and how, variations in the surface atomistic structure might introduce/eliminate electronic trap states, thereby governing the primary physical properties, foremost the PL QYs. In Figure 3, we illustrate aging of a fully capped 3.6 nm $CsPbX_3$ perovskite NC, described by the formula $[CsPbX_3](PbX_2)_m\{AX'\}_n$. The ($PbX_2$) termination and {AX′} ligand shell are believed to best resemble the experimentally found surface, as explained above. In the specific example, we choose X = Br, as $CsPbBr_3$ is currently the most widely studied halide variant; due to computational advantage, we further choose A = Cs and X′ = Br. However, we verified that A = oleylammonium, the commonplace ligand, yields qualitatively similar results; the same holds for X′ = oleate, which may be present in an amine-rich environment.[9]

The initial NC is anion-rich (anion/lead = 3.50 for a 3.6 nm NC, equal to state "1" in Figure 2). The upper left structure in Figure 3a shows its geometry after structural relaxation (for the computational details, see the Supporting Information). For simplicity, a cubic $CsPbBr_3$ crystal structure was taken as a starting configuration for DFT simulations. This then relaxes to an orthorhombically distorted polymorph, as in the experiments.[82,83] The electronic structure of the valence band is shown below, where horizontal blue and red bars indicate the relative orbital contribution from the core and the surface, respectively; in this case, the surface is defined as the outermost (one atom thick) layer of the NC. For all of the depicted valence band states, the primary contribution comes from the core, suggesting proper delocalizaton over the core and a trap-free NC.

Removing a fraction x ($0 < x < 1$) of the outer {AX′} shell leads to the structure $[CsPbX_3](PbX_2)_k\{AX'\}_{n(1-x)}$. In terms of the anion/lead ratio shown in Figure 2, this means gradually moving from a maximally anion-rich structure ("state 1") toward a maximally lead-rich structure ("state 3"). We decided to strip ion pairs starting from the vertices and edge sites, followed by the center sites, as edge and vertices are more prone to ligand detachment (see Supporting Information). However, qualitatively similar trends are observed also for random removal of ligands (see Figure S2), suggesting only a minor effect of the way these ligands are removed. As shown in Figure 3a, losing up to 75% ($x = 0.75$) of the {AX′} shell largely preserves the crystalline structure; furthermore, the main orbital contribution comes from the core, for all valence band states. Only essentially full stripping of {AX′} units (i.e., $x = 1$) leads to the appearance of states localized at the surface, as illustrated by the molecular orbital plots of the valence band edge states (i.e., the HOMOs), depicted below the electronic structures in Figure 3a. These states (indicated by dashed ellipses) may act as charge-trapping sites. Given the harsh treatment, the appearance of trap states is not surprising. Rather, it is remarkable that these anion-rich, {AX′}-terminated NCs are initially fairly robust to ligand loss, with delocalized valence band states up to a loss of about three-

DOI: 10.1021/acsenergylett.8b01669
ACS Energy Lett. 2019, 4, 63−74

quarters of the entire {AX′} shell. For similar robustness of the conduction band states, see Figure S3.

In Figure 3b, we then investigated if such trap-tolerant behavior also holds for a lead-halide-terminated $[CsPbX_3]$-$(PbX_2)_k$ or uncapped $[CsPbX_3]$ NC. Continued stripping of a fraction y ($0 < y < 1$) of the now exposed (PbX_2) shell, thereby forming $[CsPbX_3](PbX_2)_{k(1-y)}$, first leads to a lead-rich (anion/lead = 2.60) and then an anion-rich structure (anion/lead = 3.95); see transitions from state "3" to state "1" in Figure 2. We note that instead of starting the aging process immediately from the final structure ($x = 1$) formed in Figure 3a, we first displace very few additional (PbX_2); see the Supporting Information for a justification of this procedure. This initial structure ($y = 0$) features the expected cubic structure and a seemingly trap-free valence band, albeit with a higher surface contribution to the orbitals. However, stripping only 25% of the ligands already leads to the appearance of a large amount of trap states at the surface (indicated by dashed ellipses and corresponding HOMO plots) and a significantly deformed geometry. The NC structure further deforms upon additional (PbX_2) stripping and additional trap states appear. In conclusion, compared to the {AX′}-capped NC, the (PbX_2)-terminated NCs seem to be more sensitive to aging-induced trap formation via ligand displacement.

Realistic aging may deviate from the ideal (sequential) pathway depicted in Figure 2 and instead proceed via simultaneous damage of the inner (PbX_2) and outer {AX′} shells; see Figure 3c. However, the general conclusions regarding the effect on electronic structure, structural reorganizations, and anion/lead ratio per loss of {AX′} or (PbX_2) ion pair remain the same.

In a simplified view, the larger tolerance toward traps or structural deformations upon loss of the {AX′} layer, as compared to the (PbX_2) layer, is not surprising. Since the electronic structure around the band edges is predominantly given by the PbX_6^{4-} octahedra, their preservation is crucial for avoiding trap states. Per {AX′} loss, only one halide is lost, yielding PbX_5^{3-} species, which still preserve the connection between the octahedra. Upon (PbX_2) loss, however, larger structural reorganization may occur, leading to unstable states at the surface. Computationally, we notice even formation of Pb_2X_6 complexes on the surface of NCs, a clear sign of a disintegration of the perovskite structure.

Having identified the likely atomistic origin of traps in perovskite NCs, we highlight the factors paramount for the retention/recovery of the trap-free surface structure. Foremost, it is critical to rebuild all damaged surface PbX_6 octahedra, i.e., to close the inner (PbX_2) shell and overcoat it with a stable {AX′} shell (Figure 3c). The latter must contain a sufficient quantity of long-chain A (e.g., alkylammonium) or X′ (e.g., carboxylate) moieties for efficient colloidal stabilization, the rest being smaller cations (e.g., Cs^+) and anions (e.g., Br^-). Hence all these small and large ions must be available in the medium for reconstructing the NC surface. For our $CsPbBr_3$ case study, an obvious path to such trap-free surfaces would be to simultaneously treat the damaged NC surface with a mixture of long-chain ligands and $PbBr_2$. Next to this, sufficient quantities of Cs^+ and Br^- must be provided as well.

Benchmark Experiments. In the following, we discuss the experimental observations on $CsPbBr_3$ NCs in the light of the aging model presented above (see Figures 2 and 3) and, on the basis of the suggested recovery (see Figure 3c), devise an effective surface treatment strategy for restoring trap-free surfaces (high PL QYs) along with the retention of colloidal integrity. The discussion is guided by a set of experiments. We also review the known experimental facts on $CsPbBr_3$ NCs and how they agree with the proposed model.

Starting Colloid. The crude solution of ca. 9 nm $CsPbBr_3$ NCs (see size histogram on Figure S4; PL peak position at around 513 nm, Figure S5), synthesized accordingly to an earlier report from some of us (Protesescu et al.;[4] oleylamine (OLA) and oleic acid (OA) as surfactants, octadecene as initial solvent; see the Supporting Information for details), was centrifuged at 12.1 krpm (20130*g* for a specific centrifuge used, *g* being the unit of the Earth's gravity) for 5 min, and the supernatant was discarded. The precipitation was redispersed in 300 μL of hexane and centrifuged again (at 10 krpm, 3 min), and the precipitate was discarded. The so-obtained solution in hexane was diluted two times and used for all experiments described below and denoted as the "starting colloid". We note that this procedure for the initial isolation and size selection of $CsPbBr_3$ is commonplace, as can be exemplified by refs 19, 46, 49, and 84. Common variants of this purification involve the use of toluene in place of hexane (in the steps described above) or addition of 1-BuOH to such toluene solutions, followed by centrifugation and redispersion;[4,38,39,47] so-called solvent/nonsolvent purification, discussed later in the text.

Effect of Dilution. Such as-synthesized NCs are expected to be coated with an OAm^+ cation and oleate and Br^- anions, forming an AX′ shell in our taxonomy. These specific ligands are known to bind dynamically and loosely, and hence are expected to desorb this ligand shell due to its dynamic binding to the NC surface.[19] In this context, we need to emphasize that QYs in this study and in the literature are mostly reported as measured in reference to dye molecules, such as Rhodamine 6G for the green-emissive NCs, obtained by comparing the integrated intensities of the emission and accounting for the absorbance at the excitation wavelengths. The protocol for such a QY measurement involves massive dilution of the sample to the optical density of typically 0.05−0.1 (1 cm path cuvette) at the absorption peak in order to minimize the reabsorption of the emitted light. For $CsPbBr_3$, this corresponds to a dilution to a level of ca. 0.03−0.04 mg/mL (with respect to the mass of $CsPbBr_3$), which is a factor of ca. 200 times lower than the concentration of the as-prepared "starting colloid". The QYs from the diluted "starting colloid" fall typically in the range of 60−70% right after dilution and further quickly drop in the course of hours to days. The undiluted "starting colloid" also fully degrades after 10 days.

Effect of Purification with Nonsolvents. Another commonplace procedure is destabilization of colloids by the addition of a nonsolvent (e.g., acetonitrile) to the "starting colloid", followed by centrifuging in order to collect NCs and redispersion in a pure solvent (e.g., toluene), here denoted as a "purified colloid". Our QY measurements after this procedure, followed by the appropriate dilution (as described above), showed QYs on the order of 8−10%. Such a detrimental effect of the nonsolvent already after the first precipitation had been reported by many other groups.[10,37,39,41] Addition of the ligands (OLA + OA) along with the nonsolvent, with the aim to suppress the ligand desorption, had only a marginal positive effect on the QYs (reaching 30−40% at best) and shelf life of the colloids. We thus conclude that standard procedures such as addition of nonsolvents or dilution all render $CsPbBr_3$ NC surfaces moderately or heavily damaged.

DOI: 10.1021/acsenergylett.8b01669
ACS Energy Lett. 2019, 4, 63−74

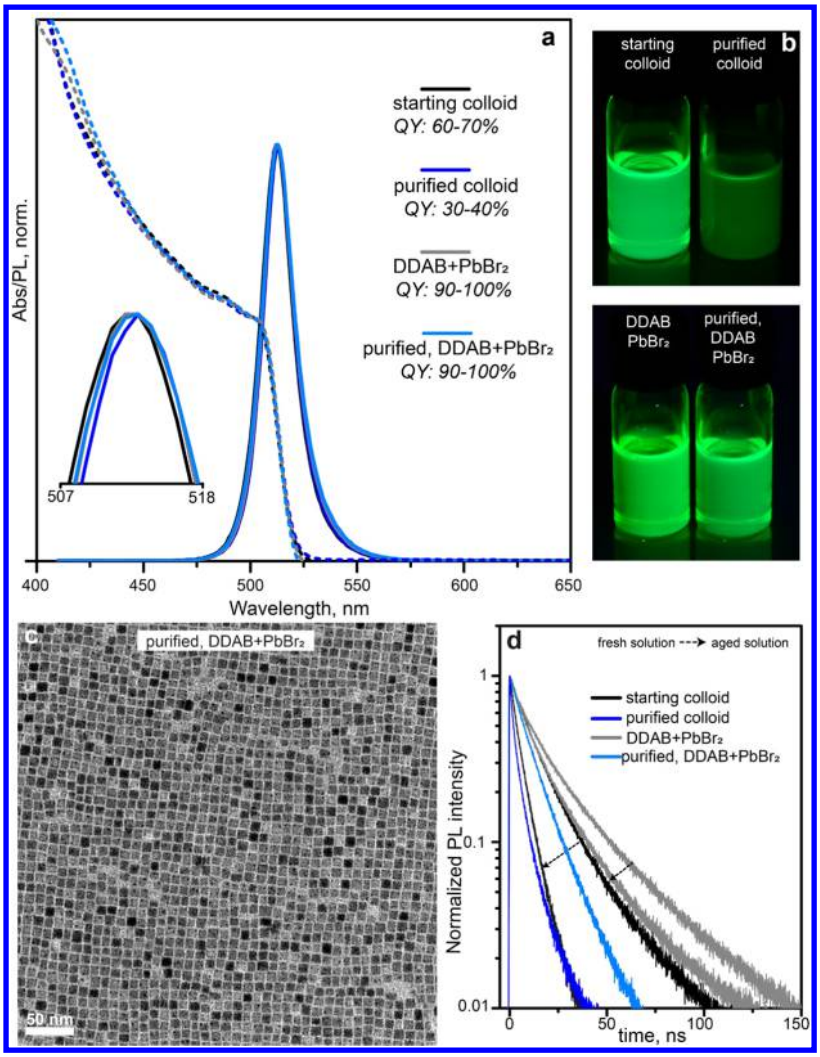

Figure 4. (a) Comparison of the steady-state absorption and PL spectra for the starting colloid and the same colloid subjected to several treatments (for details see sample numbers 1, 2, 9, and 11 in the Supporting Information): untreated starting colloid of OLA/OA-stabilized NCs (black line, sample 1), starting colloid precipitated with the acetone as a nonsolvent (containing OLA and OA) and redispersed in toluene (dark blue line, sample 2), starting colloid treated with the mixture of DDAB + $PbBr_2$ (gray line, sample 9), and purified colloid (sample 2) treated with the mixture of DDAB + $PbBr_2$ (blue line, sample 11). The inset magnifies the PL peak region. All colloids have been colloidally stable and their visual brightness under UV irradiation (see (b)) clearly reflected the variation of the measured QYs. (c) TEM image of sample 11, indicating the retention of structural integrity. (d) TRPL spectra for the same samples. For samples 1 and 9, the effect of aging by several days is indicated by dashed arrows.

DDAB + $PbBr_2$ Treatment for Surface Restoration. Herein we find that an efficient postsynthesis surface treatment for maximizing the QYs and durability of $CsPbBr_3$ NCs was treatment of the "starting colloid" that invokes didodecyldimethylammonium bromide (DDAB). The obvious advantage of the DDA cations and other quaternary ammonium salts is that their charged state is pH-independent (unlike OAmBr). The DDA cation had long been known as an excellent former of stable hydrophobic monolayers, either as free-standing molecular aggregates (used, for instance, as templates for growing mesostructured silica[85,86]) or for functionalization (hydrophobization) of negatively charged surfaces such as those of aluminosilicates (forming so-called organoclays)[87−90] and anion-capped metal chalcogenide NCs.[91] DDA and other molecules with two long hydrocarbon chains ($2C_n$) are known to form more stable monolayers due to a good match between the molecule cross section and the typical densities of negatively charged surface sites. Importantly, longer chains ($\geq C_{16}$) often render the alkylammonium salts insoluble in typical apolar solvents.

The idea of adding $PbBr_2$ together with DDAB stems directly from the theory presented above—it might be able to rebuild the damaged $PbBr_6$ octahedra. Importantly, we note that in the NC, the Pb:Br ratio has to be at least 1:3. Hence the combination of DDAB + $PbBr_2$ appears better than using $PbBr_2$ alone. We note that $PbBr_2$ alone is not soluble in toluene but quickly and fully dissolves upon addition of DDAB, forming an adduct, presumably $DDAPbBr_3$ and/or DDA_2PbBr_4. Addition of DDAB alone or better DDAB + $PbBr_2$ (in 2:1 molar ratio) was able to recover the QYs to the level of 90−100% (Figure 4). The actually measured values in this case often exceed 100% by a few percent, which is understandable considering the estimated systematic measurement error of ±5%. Such dramatic recovery of QYs to near 100% was observed for "starting colloids" (QY = 60−70%) and for colloids treated by nonsolvents (QYs = 30−40%,

DOI: 10.1021/acsenergylett.8b01669
ACS Energy Lett. 2019, 4, 63−74

depending upon the used nonsolvent and dilution). In comparison with NCs treated only with DDAB, a combined DDAB + $PbBr_2$ treatment systematically yielded 10−20%-higher QYs and longer shelf life (e.g., the first signs of agglomeration appear at least four months later). NCs treated with DDAB + $PbBr_2$ can sustain multiple steps, at least three, of precipitation and redispersion (with ethyl acetate, 2-propanol, acetone, and acetonitrile as nonsolvents and toluene as a solvent). Such rigorous washing procedures are not applicable to the "starting colloid", which is rendered insoluble already after the first round of such washing. This observation further highlights the robustness of the DDAB coating. The dilution has an apparently negligible effect, evident from a long shelf life of diluted colloids and retention of a high QY during storage. We find that addition of OA as a coligand to DDAB or DDAB + $PbBr_2$ has a rather detrimental effect, manifested in a rather rapid drop of the QY during storage (by a factor of 2 after 5 days). In fact, earlier studies on OLA/OA-stabilized $CsPbBr_3$ NCs have pointed out that the oleate ion is rather absent at the NC surface, and the role of OA is rather to protonate OLA.[19,56] This indicates that OA is not needed for quaternary ammonium salts as capping agents.

Reference Experiments (Figures S5 and S6). We have conducted also a set of reference experiments to delineate individual effects of various reagents. In the footstep of the report by Alivisatos et al.,[22] addition of NH_4SCN powder (this salt is not soluble in toluene) to the "starting colloid" yielded an improvement of the QY from below 70% to 80−85% (100% in ref 22). Similarly to Alivisatos et al.,[22] we have observed a slight blue shift (ca. 2 nm, or 10 meV), which can be explained by the removal of the surface Pb atoms from the damaged $PbBr_2$ layer upon coordination with SCN^-. Such removal had been also suggested by Alivisatos et al.[22] on the basis of the XPS analysis that showed an increase in the Br:Pb ratio after the treatment (from 2.74 to 3.03). As another reference experiment, we have attempted a treatment with powdered $PbBr_2$ (essentially insoluble in toluene) without an observable effect on PL QYs or long-term colloidal stability. We also treated the "starting colloid" with a mixture of $PbBr_2$−OA−OLA, as previously proposed for NC films,[25] and this had not been effective for colloidal NCs.

Overall, the surface treatments described in our study had rather minor effects on the PL peak wavelengths (512−514 nm) or PL fwhm (18−20 nm) as well as absorption spectra (see Figure 4a and, for a broader overview of various samples, Figures S5 and S6). Shifting PL peaks by no more than 1−2 nm to the blue or red side can be attributed to either removal or restoration of the outermost $PbBr_2$ layer. Hence, on the basis of the minute changes to the absorption and PL spectra, we exclude deep etching or restructuring of NCs, in line with TEM images which lack noticeable changes to the NCs size and shape (see Figures 4c and S7).

On the basis of the experiments above, and in full consistency with the proposed theory, the treatment by the mixture of DDAB (acting as a ligand) and $PbBr_2$ (for repairing the Pb−Br layer), more correctly by their adduct, had been the only effective path to reach near-unity QYs and long-term colloidal durability, the latter being the ability to retain high PL QYs upon multiple solvent/nonsolvent purification steps.

Time-Resolved PL. The obtained time-resolved PL decays corroborate the conclusions drawn thus far (see Figure 4d and, for a broader overview, Tables S2 and S3 and Figures S8 and S9). Longer intensity-averaged lifetimes (extracted from biexponential fits; see Table S2) correlate well with higher QYs: upon passivation, the faster nonradiative decay component decreases, whereas the longer lived, radiative bimolecular recombination enhances. While fresh "starting colloids" (black line in Figure 4d) show an average lifetime of 19 ns and QYs of 60−70%, these parameters decrease to 6.5 ns and 30−40%, respectively, after storage for 2 weeks. A similarly detrimental effect on the average PL lifetime is seen after purification with the nonsolvent (dark blue line). When the latter is subjected to DDAB-$PbBr_2$ treatment (light blue line), the average PL lifetimes double. The slowest PL decay, in 28.2 ns, is observed for the same "starting colloid" after being subjected to DDAB-$PbBr_2$ treatment (gray line); this PL decay only moderately accelerates after 2 weeks of storage. Furthermore, intense purification of such DDAB-$PbBr_2$-treated samples by repetitive precipitation with ethyl acetate (or acetone) and redispersion in toluene, by up to 3 times, did not substantially affect the time-resolved PL decays (Figure S8) and QYs (remained above 90%). We should also note that, on the basis of numerous studied samples, we have not found a correlation between the single-exponential-decay behavior and QYs. In fact, nearly all PL decay traces remained nonsingle-exponential. Instead, we find that PL decay traces evolve toward single-exponential when the PL collection wavelengths is set to the longer wavelengths shoulder of the PL band (Figure S9), suggesting that energy transfer or photon recycling within the ensemble of colloidal NCs may contribute to the observed decay kinetics. This matter requires further detailed study.

Comments on Relevant Results from the Literature. Herein we try to draw some conclusions also with the existing literature. We must note that the accurate comparison with the $[CsPbX_3](PbX_2)_k[AX']_n$ model and with our experiments summarized above is virtually impossible for a number of reasons, foremost because of a complex interplay of various factors and cross-effects of different reagents and, occasionally, lack of details or differences in the experimental protocols (such as for QY measurements). However, certain qualitative conclusions can be drawn.

Bakr et al. reported that the treatment of solution similar to our "starting colloid" with DDA sulfide (DDAS) resulted in an increase of the PL QYs by up to a factor of 2 (to ca. 70%) and improved long-term stability.[47] Similar improvements after DDAS treatment were reported also by others, for instance, in ref 81. Later on the focus shifted toward DDAB-based treatments: Bakr et al. reported on the mixed DDAB-OA treatment to yield improved QYs of 70% and LEDs with the EQE of 1.9% (and luminance of 35 cd m^{-2}),[38] commensurate with that of DDAS treatment in their earlier study.[47] Interestingly, the same study pointed to a substantial QY drop when $CsPbBr_3$ NCs were treated with OA only,[38] in agreement with our observations. Other reports also point to the detrimental effects of the treatments with increased concentrations of carboxylic acids or when the acid is a sole capping/treating agent.[25] Kido et al. also studied DDAB-OA treatments, varying the choice of the nonsolvent (BuOH, AcOEt, AcOBu, MeCN, 2-propanol) used before and after the addition of the DDAB-OA mixture,[39] achieving PL QYs of 70−80% in solution and demonstrating LEDs with external quantum efficiencies of 8.73%. Even higher EQE values of up to 11.6% have been reported with $CsPbBr_3$ NCs synthesized using a multiligand system, containing DDAB.[15] Yang et al.[92] used a mixture of oleylammonium bromide and lead oleate for

DOI: 10.1021/acsenergylett.8b01669
ACS Energy Lett. 2019, 4, 63−74

improving the PL QY of $CsPbBr_3$ nanowires to ca. 50%. Overall, the $[CsPbX_3](PbX_2)_k[AX']_n$ model is consistent with all known studies; in particular, Nag et al. recently elucidated the surface chemistry of OLA/OA-synthesized $CsPbBr_3$ NCs by combining XPS, NMR, and DFT and arriving at similar conclusions as to CsBr termination with partial substitution of Cs^+ with OLA cations.[56]

As to the closely related $CsPbI_3$ NCs, quite intriguing is the effective enhancement of PL QYs of $CsPbI_3$ to 30−100% and substantial delay of the phase transition into a nonperovskite phase (a characteristic issue of this iodide) after treatment with trioctylphosphine.[68,72,93] We can attribute such treatment to Lewis acid−base (TOP being Lewis base; for instance, TOP can dissolve PbX_2 into apolar solvents) interaction with undercoordinated Pb atoms at the NCs surface, leading either to coordination of TOP to the NC surface (as experimentally implied in ref 68) or to the removal of such an adduct from the NC surface (thus restoring the NC "closed shells", similarly to the thiocyanate treatment). Similar effects (increased PLQYs and longer radiative lifetimes) were observed also from the thin films of $MAPbI_3$ treated with TOP or other Lewis acids.[94]

Highly relevant are also observations on the PL behavior of polycrystalline perovskite thin films, used in photovoltaics and light-emitting devices. Stranks et al. have recently shown that K halide termination at the surfaces or grain boundaries of $(Cs,FA,MA)Pb(I_{0.85}Br_{0.15})_3$ films led to external PL QYs of 66%, which, together with accounting for photon recycling and light-out-coupling effects, give internal yields exceeding 95%.[95]

Utility of ICP-OES and XPS for Monitoring the Anion/Lead Ratio: Experiment and Discussion. ICP-OES provides an overall chemical composition of NCs, thus being the most relevant tool for testing the compositional predictions outlined in Figures 1 and 2. XPS, on the contrary, probes only the surface region, typically up to 2 nm in depth (see the sketch in Figure S10). The signal collection depths with XPS is also element-specific and depends on the presence and density of the surface capping ligands etc. Hence it is natural to expect that ICP-OES and XPS may yield quantitatively different results. XPS by no means can be expected to reflect the overall stoichiometry of the sample but should rather be used to probe relative changes in the surface composition in response to various surface treatments or processing conditions. We suggest that Rutherford backscattering spectrometry (RBS) is a method that may be advantageous over ICP-MS, ICP-OES, or XPS for the quantitative elemental analysis of NCs;[20] its only shortcoming is its generally lower availability at most institutions.

We have carried out ICP-OES analysis for $CsPbBr_3$ NCs with different surface ligands or treatments. In satisfactory agreement with Figures 1 and 2, conventional OLA/OA-capped, ∼9 nm $CsPbBr_3$ NCs, and the same NCs treated with DDAB or DDAB/$PbBr_2$ and properly purified from the excess of ligands all exhibit Br/Pb ratios above 3, typically 3.2−3.5, in agreement with the conclusion that OLA and DDA cations are the dominant long-chain organic species in these NCs, charge balanced with Br^-. We note that some of the excessive Br might originate from the residual ligand too. On the contrary, zwitterionic-ligand-capped $CsPbBr_3$ NCs, synthesized as reported by us earlier,[10] all exhibit Br/Pb ratios below 3 (typically 2.6−2.9). In such NCs, one expects that the {AX′} layer is rather made of zwitterionic ligands and hence is rather Br-poor. We also note that we have developed a special procedure for the sample preparation for ICP-OES, which is rather well suited for all $APbX_3$ NCs (see the Supporting Information for details). Therein, we omitted using oxidative digestive solutions, as these led to the loss of halide (as volatile X_2). Instead, $CsPbBr_3$ NCs were ionically dissolved in a polar solvent, an aqueous HCl solution, that can solubilize both the core $CsPbBr_3$ and ligands (DDAB, zwitterionic, both forming molecular micelles in water).

The survey XPS spectra confirm the presence of Cs, Pb, Br, N, C, and O in the samples. The latter three are also common contaminants in conventional XPS procedures for organic-capped NCs. Thus, we focus on discussing the other elements, using quantitative analysis of higher resolution spectra for each element (Figures S11 and S12). We emphasize that, with the signal collection depth with the benchtop XPS being limited to ca. 2 nm, one should not expect any quantitative match with the theoretical $CsPbBr_3$ stoichiometry or overall stoichiometric deviation presented in Figures 1 and 2. It is rather the relative trends between the samples that makes the most sense. Our spectra are also similar to those reported in the literature.[38]

The N 1s core level is presented as a single peak, whose energy correlates with the chemical identity of the N-containing species: 402.5 eV for "starting colloid" purified by acetonitrile [sample (3), ligand OLA], 403.2−403.5 eV for DDAB-treated NCs [samples (7, 9), OLA cation displaced with DDA] and 400.4 eV for a reference sample of $FAPbBr_3$ single crystals. Reference $CsPbBr_3$ single crystals showed no signal from N 1s, confirming that the signal quantitatively originates from the sample. Interestingly, the N 1s/Pb 4f signal ratio is close to the expected value of 2 (FA contains two N atoms) for the $FAPbBr_3$ signal, and an order of magnitude lower for $CsPbBr_3$ NCs.

With Br/Pb XPS ratios (Table S4), the general trend is that this ratio is close to that obtained with $CsPbBr_3$ and $FAPbBr_3$ bulk reference samples. Most of the reports in the literature compare intensity ratios between Br 3d and Pb 4f signals and report values that are equal to or higher than 3 (3−3.2)[22,56,66,93] and lower than 3 (down to 2.9).[22,28,58,66] In our case, these values are in the range 2.91−2.99 for DDAB-treated NCs [samples (7 and 9)], 2.86 for a bulk $CsPbBr_3$ single crystal, and 2.96 for a $FAPbBr_3$ single crystal. We also note that the Br/Pb ratios determined from another core level (Br 3p) are by lower ca. 20%. We also note that there is no obvious reason to assume that the Br 3d signal is more appropriate to choose; on the contrary, Br 3p is spectrally closer to Pb 4f and thus correction factors are not as significant. As to Cs/Pb ratios, all values substantially exceed unity (by 20−50%), regardless of which Cs core level is taken into consideration (Cs 3d or Cs 4d). This highlights the inherent uncertainty about the signal collection depth with XPS. DDAB-treated samples all exhibit Cs/Pb ratios that are by just 1−5% smaller than for bulk $CsPbBr_3$. For sample 3 (purified by acetonitrile), slight increases in the Br 3d/Pb 4f ratio to 3.12 and Cs 3d/Pb 4f to 1.41 were observed, possibly indicating a preferential loss and damage of the $PbBr_2$ shell and surface enrichment with CsBr.

It is also important to point out that we have not observed any sign of deep structural transformation on the basis of XPS, ICP, and optical characterization. In principle, $CsPbX_3$ can fully or partially convert into CsX, $CsPb_2Br_5$, and Cs_4PbX_6 NCs by adding or eliminating CsX or PbX_2 units, with the aid of strongly coordinating ligands and/or highly polar solvents.[57−63,65] These transformations have not been detected after the treatments discussed in this work.

DOI: 10.1021/acsenergylett.8b01669
ACS Energy Lett. 2019, 4, 63−74

Conclusions. We propose an atomistic mechanism for the processing- or aging-induced surface damage of colloidal $CsPbX_3$ (X = Cl, Br, I) NCs. With the example of $CsPbBr_3$ NCs, we rationalize the formation of trap states, corroborated by DFT simulations and validated by the experiment (elemental analysis and optical measurements). Healing of the surface trap states requires restoration of all damaged PbX_6 octahedra and establishing a stable outer AX′ shell with cationic (A) and anionic (X′) ligands forming a core−inner shell−outer shell NC structure depicted as $[CsPbX_3](PbX_2)$-{AX′}. Such NCs are halogen-rich when X′ is largely made of X ions, and halogen-poor when other anions assume the positions of X′. Restoration of such a structure, seen as an increase in the PL QY to 90−100% and improvement in the overall robustness of $CsPbBr_3$ NCs, was attained using a facile postsynthetic treatment with a $PbBr_2$ + DDAB mixture. This model is consistent with typical observations on the PL properties of perovskite thin films as well. Future work should focus on the effective engineering of trap-free core−shell morphologies, sufficiently robust for dispersing perovskite NCs in aqueous media and for enabling thermal processing without NC sintering.

■ ASSOCIATED CONTENT

Supporting Information

The Supporting Information is available free of charge on the ACS Publications website at DOI: 10.1021/acsenergylett.8b01669.

Computational details (including figures of influence of achieving charge balance on the anion/lead ratio and of the geometry and electronic structure of $CsPbX_3$ NCs, table of band gap values); synthesis, isolation, surface treatments and optical characterization (including size histogram from TEM images, absorption, photoluminescence, and TRPL spectra, photos of the vials with the colloidal solutions, TEM images, tables of fitting results); ICP-OES and XPS analysis (including a table of composition analysis) (PDF)

■ AUTHOR INFORMATION

Corresponding Authors

*M. V. Kovalenko. E-mail: mvkovalenko@ethz.ch.
*I. Infante. E-mail: iinfant76@gmail.com.

ORCID

Maryna I. Bodnarchuk: 0000-0001-6597-3266
Simon C. Boehme: 0000-0002-8399-5773
Yevhen Shynkarenko: 0000-0002-1587-1752
Maksym V. Kovalenko: 0000-0002-6396-8938
Ivan Infante: 0000-0003-3467-9376

Notes

The authors declare no competing financial interest.

■ ACKNOWLEDGMENTS

This work was financially supported by the European Union through the FP7 (ERC Starting Grant NANOSOLID, GA No. 306733), by the Swiss Federal Commission for Technology and Innovation (CTI-No. 18614.1 PFNM-NM). M.I.B. acknowledges financial support from the Swiss National Foundation (SNF Ambizione Energy Grant No. PZENP2_154287). I.I. acknowledges The Netherlands Organization of Scientific Research (NWO) for financial support through the Innovational Research Incentive (Vidi) Scheme (Grant No. 723.013.002) and S.C.B. for financial support through the Innovational Research Incentives (Veni) Scheme (Grant No. 722.017.011). The computational work was carried out on the Dutch national e-infrastructure with the support of the SURF Cooperative. The authors are grateful to Empa Electron Microscopy Center for access to the instruments and for technical assistance.

■ REFERENCES

(1) Boles, M. A.; Ling, D.; Hyeon, T.; Talapin, D. V. The Surface Science of Nanocrystals. *Nat. Mater.* **2016**, *15*, 141−153.
(2) Talapin, D. V.; Lee, J.-S.; Kovalenko, M. V.; Shevchenko, E. V. Prospects of Colloidal Nanocrystals for Electronic and Optoelectronic Applications. *Chem. Rev.* **2010**, *110* (1), 389−458.
(3) Deringer, V. L.; Dronskowski, R. From Atomistic Surface Chemistry to Nanocrystals of Functional Chalcogenides. *Angew. Chem., Int. Ed.* **2015**, *54* (51), 15334−15340.
(4) Protesescu, L.; Yakunin, S.; Bodnarchuk, M. I.; Krieg, F.; Caputo, R.; Hendon, C. H.; Yang, R. X.; Walsh, A.; Kovalenko, M. V. Nanocrystals of Cesium Lead Halide Perovskites ($CsPbX_3$, X = Cl, Br, and I): Novel Optoelectronic Materials Showing Bright Emission with Wide Color Gamut. *Nano Lett.* **2015**, *15* (6), 3692−3696.
(5) Kovalenko, M. V.; Protesescu, L.; Bodnarchuk, M. I. Properties and Potential Optoelectronic Applications of Lead Halide Perovskite Nanocrystals. *Science* **2017**, *358* (6364), 745−750.
(6) Akkerman, Q. A.; Rainò, G.; Kovalenko, M. V.; Manna, L. Genesis, Challenges and Opportunities for Colloidal Lead Halide Perovskite Nanocrystals. *Nat. Mater.* **2018**, *17* (5), 394−405.
(7) Zhang, Q.; Yin, Y. All-Inorganic Metal Halide Perovskite Nanocrystals: Opportunities and Challenges. *ACS Cent. Sci.* **2018**, *4* (6), 668−679.
(8) Kovalenko, M. V.; Bodnarchuk, M. I. Lead Halide Perovskite Nanocrystals: From Discovery to Self-assembly and Applications. *Chimia* **2017**, *71* (7−8), 461−470.
(9) ten Brinck, S.; Infante, I. Surface Termination, Morphology, and Bright Photoluminescence of Cesium Lead Halide Perovskite Nanocrystals. *ACS Energy Lett.* **2016**, *1* (6), 1266−1272.
(10) Krieg, F.; Ochsenbein, S. T.; Yakunin, S.; ten Brinck, S.; Aellen, P.; Süess, A.; Clerc, B.; Guggisberg, D.; Nazarenko, O.; Shynkarenko, Y.; et al. Colloidal $CsPbX_3$ (X = Cl, Br, I) Nanocrystals 2.0: Zwitterionic Capping Ligands for Improved Durability and Stability. *ACS Energy Lett.* **2018**, *3* (3), 641−646.
(11) Imran, M.; Caligiuri, V.; Wang, M.; Goldoni, L.; Prato, M.; Krahne, R.; De Trizio, L.; Manna, L. Benzoyl Halides as Alternative Precursors for the Colloidal Synthesis of Lead-Based Halide Perovskite Nanocrystals. *J. Am. Chem. Soc.* **2018**, *140* (7), 2656−2664.
(12) Levchuk, I.; Osvet, A.; Tang, X.; Brandl, M.; Perea, J. D.; Hoegl, F.; Matt, G. J.; Hock, R.; Batentschuk, M.; Brabec, C. J. Brightly Luminescent and Color-Tunable Formamidinium Lead Halide Perovskite $FAPbX_3$ (X = Cl, Br, I) Colloidal Nanocrystals. *Nano Lett.* **2017**, *17* (5), 2765−2770.
(13) Vybornyi, O.; Yakunin, S.; Kovalenko, M. V. Polar-Solvent-Free Colloidal Synthesis of Highly Luminescent Alkylammonium Lead Halide Perovskite Nanocrystals. *Nanoscale* **2016**, *8* (12), 6278−6283.
(14) Weidman, M. C.; Seitz, M.; Stranks, S. D.; Tisdale, W. A. Highly Tunable Colloidal Perovskite Nanoplatelets through Variable Cation, Metal, and Halide Composition. *ACS Nano* **2016**, *10* (8), 7830−7839.
(15) Song, J.; et al. Room-Temperature Triple-Ligand Surface Engineering Synergistically Boosts Ink Stability, Recombination Dynamics, and Charge Injection toward EQE-11.6% Perovskite QLEDs. *Adv. Mater.* **2018**, *30*, 1800764.
(16) Akkerman, Q. A.; Gandini, M.; Di Stasio, F.; Rastogi, P.; Palazon, F.; Bertoni, G.; Ball, J. M.; Prato, M.; Petrozza, A.; Manna, L. Strongly Emissive Perovskite Nanocrystal Inks for High-Voltage Solar Cells. *Nat. Energy* **2017**, *2*, 16194.

DOI: 10.1021/acsenergylett.8b01669
ACS Energy Lett. 2019, 4, 63−74

(17) Zhang, D.; Eaton, S. W.; Yu, Y.; Dou, L.; Yang, P. Solution-Phase Synthesis of Cesium Lead Halide Perovskite Nanowires. *J. Am. Chem. Soc.* **2015**, *137* (29), 9230−9233.
(18) Dutta, A.; Dutta, S. K.; Das Adhikari, S.; Pradhan, N. Tuning the Size of $CsPbBr_3$ Nanocrystals: All at One Constant Temperature. *ACS Energy Lett.* **2018**, *3* (2), 329−334.
(19) De Roo, J.; Ibanez, M.; Geiregat, P.; Nedelcu, G.; Walravens, W.; Maes, J.; Martins, J. C.; Van Driessche, I.; Kovalenko, M. V.; Hens, Z. Highly Dynamic Ligand Binding and Light Absorption Coefficient of Cesium Lead Bromide Perovskite Nanocrystals. *ACS Nano* **2016**, *10* (2), 2071−2081.
(20) Maes, J.; Balcaen, L.; Drijvers, E.; Zhao, Q.; De Roo, J.; Vantomme, A.; Vanhaecke, F.; Geiregat, P.; Hens, Z. Light Absorption Coefficient of $CsPbBr_3$ Perovskite Nanocrystals. *J. Phys. Chem. Lett.* **2018**, *9* (11), 3093−3097.
(21) Yang, D.; et al. Surface Chemistry of All Inorganic Halide Perovskite Nanocrystals: Passivation Mechanism and Stability. *Adv. Mater. Interfaces* **2018**, *5* (8), 1701662.
(22) Koscher, B. A.; Swabeck, J. K.; Bronstein, N. D.; Alivisatos, A. P. Essentially Trap-Free $CsPbBr_3$ Colloidal Nanocrystals by Postsynthetic Thiocyanate Surface Treatment. *J. Am. Chem. Soc.* **2017**, *139* (19), 6566−6569.
(23) Pan, J.; Shang, Y.; Yin, J.; De Bastiani, M.; Peng, W.; Dursun, I.; Sinatra, L.; El-Zohry, A. M.; Hedhili, M. N.; Emwas, A.-H.; et al. Bidentate Ligand-Passivated $CsPbI_3$ Perovskite Nanocrystals for Stable Near-Unity Photoluminescence Quantum Yield and Efficient Red Light-Emitting Diodes. *J. Am. Chem. Soc.* **2018**, *140* (2), 562−565.
(24) Wheeler, L. M.; Sanehira, E. M.; Marshall, A. R.; Schulz, P.; Suri, M.; Anderson, N. C.; Christians, J. A.; Nordlund, D.; Sokaras, D.; Kroll, T.; et al. Targeted Ligand Exchange Chemistry on Cesium Lead Halide Perovskite Quantum Dots for High-Efficiency Photovoltaics. *J. Am. Chem. Soc.* **2018**, *140* (33), 10504−10513.
(25) Di Stasio, F.; Christodoulou, S.; Huo, N.; Konstantatos, G. Near-Unity Photoluminescence Quantum Yield in $CsPbBr_3$ Nanocrystal Solid-State Films via Postsynthesis Treatment with Lead Bromide. *Chem. Mater.* **2017**, *29* (18), 7663−7667.
(26) Bohn, B. J.; Tong, Y.; Gramlich, M.; Lai, M. L.; Döblinger, M.; Wang, K.; Hoye, R. L. Z.; Müller-Buschbaum, P.; Stranks, S. D.; Urban, A. S.; et al. Boosting Tunable Blue Luminescence of Halide Perovskite Nanoplatelets through Postsynthetic Surface Trap Repair. *Nano Lett.* **2018**, *18* (8), 5231−5238.
(27) Ahmed, T.; Seth, S.; Samanta, A. Boosting the Photoluminescence of $CsPbX_3$ (X = Cl, Br, I) Perovskite Nanocrystals Covering a Wide Wavelength Range by Postsynthetic Treatment with Tetrafluoroborate Salts. *Chem. Mater.* **2018**, *30* (11), 3633−3637.
(28) Wu, H.; Zhang, Y.; Lu, M.; Zhang, X.; Sun, C.; Zhang, T.; Colvin, V. L.; Yu, W. W. Surface Ligand Modification of Cesium Lead Bromide Nanocrystals for Improved Light-Emitting Performance. *Nanoscale* **2018**, *10* (9), 4173−4178.
(29) Ravi, V. K.; Scheidt, R. A.; Nag, A.; Kuno, M.; Kamat, P. V. To Exchange or Not to Exchange. Suppressing Anion Exchange in Cesium Lead Halide Perovskites with $PbSO_4$−Oleate Capping. *ACS Energy Lett.* **2018**, *3* (4), 1049−1055.
(30) Das Adhikari, S.; Dutta, S. K.; Dutta, A.; Guria, A. K.; Pradhan, N. Chemically Tailoring the Dopant Emission in Manganese-Doped $CsPbCl_3$ Perovskite Nanocrystals. *Angew. Chem.* **2017**, *129* (30), 8872−8876.
(31) Mir, W. J.; Jagadeeswararao, M.; Das, S.; Nag, A. Colloidal Mn-Doped Cesium Lead Halide Perovskite Nanoplatelets. *ACS Energy Lett.* **2017**, *2* (3), 537−543.
(32) Liu, H.; Wu, Z.; Shao, J.; Yao, D.; Gao, H.; Liu, Y.; Yu, W.; Zhang, H.; Yang, B. $CsPb_xMn_{1-x}Cl_3$ Perovskite Quantum Dots with High Mn Substitution Ratio. *ACS Nano* **2017**, *11* (2), 2239−2247.
(33) van der Stam, W.; Geuchies, J. J.; Altantzis, T.; van den Bos, K. H. W.; Meeldijk, J. D.; Van Aert, S.; Bals, S.; Vanmaekelbergh, D.; de Mello Donega, C. Highly Emissive Divalent-Ion-Doped Colloidal $CsPb_{1-x}M_xBr_3$ Perovskite Nanocrystals through Cation Exchange. *J. Am. Chem. Soc.* **2017**, *139* (11), 4087−4097.
(34) Yuan, X.; Ji, S.; De Siena, M. C.; Fei, L.; Zhao, Z.; Wang, Y.; Li, H.; Zhao, J.; Gamelin, D. R. Photoluminescence Temperature Dependence, Dynamics, and Quantum Efficiencies in Mn^{2+}-Doped $CsPbCl_3$ Perovskite Nanocrystals with Varied Dopant Concentration. *Chem. Mater.* **2017**, *29* (18), 8003−8011.
(35) Milstein, T. J.; Kroupa, D. M.; Gamelin, D. R. Picosecond Quantum Cutting Generates Photoluminescence Quantum Yields Over 100% in Ytterbium-Doped $CsPbCl_3$ Nanocrystals. *Nano Lett.* **2018**, *18* (6), 3792−3799.
(36) Zhou, Q.; Bai, Z.; Lu, W. G.; Wang, Y.; Zou, B.; Zhong, H. In Situ Fabrication of Halide Perovskite Nanocrystal-Embedded Polymer Composite Films with Enhanced Photoluminescence for Display Backlights. *Adv. Mater.* **2016**, *28* (41), 9163−9168.
(37) Tan, Y.; Zou, Y.; Wu, L.; Huang, Q.; Yang, D.; Chen, M.; Ban, M.; Wu, C.; Wu, T.; Bai, S.; et al. Highly Luminescent and Stable Perovskite Nanocrystals with Octylphosphonic Acid as a Ligand for Efficient Light-Emitting Diodes. *ACS Appl. Mater. Interfaces* **2018**, *10* (4), 3784−3792.
(38) Pan, J.; Quan, L. N.; Zhao, Y.; Peng, W.; Murali, B.; Sarmah, S. P.; Yuan, M.; Sinatra, L.; Alyami, N. M.; Liu, J.; et al. Highly Efficient Perovskite-Quantum-Dot Light-Emitting Diodes by Surface Engineering. *Adv. Mater.* **2016**, *28* (39), 8718−8725.
(39) Chiba, T.; Hoshi, K.; Pu, Y. J.; Takeda, Y.; Hayashi, Y.; Ohisa, S.; Kawata, S.; Kido, J. High-Efficiency Perovskite Quantum-Dot Light-Emitting Devices by Effective Washing Process and Interfacial Energy Level Alignment. *ACS Appl. Mater. Interfaces* **2017**, *9* (21), 18054−18060.
(40) Deng, W.; Xu, X.; Zhang, X.; Zhang, Y.; Jin, X.; Wang, L.; Lee, S.-T.; Jie, J. Organometal Halide Perovskite Quantum Dot Light-Emitting Diodes. *Adv. Funct. Mater.* **2016**, *26* (26), 4797−4802.
(41) Li, J.; Xu, L.; Wang, T.; Song, J.; Chen, J.; Xue, J.; Dong, Y.; Cai, B.; Shan, Q.; Han, B.; et al. 50-Fold EQE Improvement up to 6.27% of Solution-Processed All-Inorganic Perovskite $CsPbBr_3$ QLEDs via Surface Ligand Density Control. *Adv. Mater.* **2017**, *29* (5), 1603885.
(42) Li, G.; Rivarola, F. W.; Davis, N. J.; Bai, S.; Jellicoe, T. C.; de la Pena, F.; Hou, S.; Ducati, C.; Gao, F.; Friend, R. H.; et al. Highly Efficient Perovskite Nanocrystal Light-Emitting Diodes Enabled by a Universal Crosslinking Method. *Adv. Mater.* **2016**, *28* (18), 3528−3534.
(43) Zhang, X.; Sun, C.; Zhang, Y.; Wu, H.; Ji, C.; Chuai, Y.; Wang, P.; Wen, S.; Zhang, C.; Yu, W. W. Bright Perovskite Nanocrystal Films for Efficient Light-Emitting Devices. *J. Phys. Chem. Lett.* **2016**, *7* (22), 4602−4610.
(44) Swarnkar, A.; Marshall, A. R.; Sanehira, E. M.; Chernomordik, B. D.; Moore, D. T.; Christians, J. A.; Chakrabarti, T.; Luther, J. M. Quantum Dot−Induced Phase Stabilization of α-$CsPbI_3$ Perovskite for High-Efficiency Photovoltaics. *Science* **2016**, *354* (6308), 92−95.
(45) Sanehira, E. M.; Marshall, A. R.; Christians, J. A.; Harvey, S. P.; Ciesielski, P. N.; Wheeler, L. M.; Schulz, P.; Lin, L. Y.; Beard, M. C.; Luther, J. M. Enhanced Mobility $CsPbI_3$ Quantum Dot Arrays for Record-Efficiency, High-Voltage Photovoltaic Cells. *Sci. Adv.* **2017**, *3* (10), eaao4204.
(46) Yakunin, S.; Protesescu, L.; Krieg, F.; Bodnarchuk, M. I.; Nedelcu, G.; Humer, M.; De Luca, G.; Fiebig, M.; Heiss, W.; Kovalenko, M. V. Low-Threshold Amplified Spontaneous Emission and Lasing from Colloidal Nanocrystals of Caesium Lead Halide Perovskites. *Nat. Commun.* **2015**, *6*, 8056.
(47) Pan, J.; Sarmah, S. P.; Murali, B.; Dursun, I.; Peng, W.; Parida, M. R.; Liu, J.; Sinatra, L.; Alyami, N.; Zhao, C.; et al. Air-Stable Surface-Passivated Perovskite Quantum Dots for Ultra-Robust, Single- and Two-Photon-Induced Amplified Spontaneous Emission. *J. Phys. Chem. Lett.* **2015**, *6* (24), 5027−5033.
(48) Becker, M. A.; Vaxenburg, R.; Nedelcu, G.; Sercel, P. C.; Shabaev, A.; Mehl, M. J.; Michopoulos, J. G.; Lambrakos, S. G.; Bernstein, N.; Lyons, J. L.; et al. Bright Triplet Excitons in Caesium Lead Halide Perovskites. *Nature* **2018**, *553*, 189.
(49) Rainò, G.; Nedelcu, G.; Protesescu, L.; Bodnarchuk, M. I.; Kovalenko, M. V.; Mahrt, R. F.; Stöferle, T. Single Cesium Lead

DOI: 10.1021/acsenergylett.8b01669
ACS Energy Lett. 2019, 4, 63−74

Halide Perovskite Nanocrystals at Low Temperature: Fast Single-Photon Emission, Reduced Blinking, and Exciton Fine Structure. *ACS Nano* **2016**, *10* (2), 2485−2490.
(50) Makarov, N. S.; Guo, S.; Isaienko, O.; Liu, W.; Robel, I.; Klimov, V. I. Spectral and Dynamical Properties of Single Excitons, Biexcitons, and Trions in Cesium−Lead-Halide Perovskite Quantum Dots. *Nano Lett.* **2016**, *16* (4), 2349−2362.
(51) Fu, M.; Tamarat, P.; Huang, H.; Even, J.; Rogach, A. L.; Lounis, B. Neutral and Charged Exciton Fine Structure in Single Lead Halide Perovskite Nanocrystals Revealed by Magneto-optical Spectroscopy. *Nano Lett.* **2017**, *17* (5), 2895−2901.
(52) Pfingsten, O.; Klein, J.; Protesescu, L.; Bodnarchuk, M. I.; Kovalenko, M. V.; Bacher, G. Phonon Interaction and Phase Transition in Single Formamidinium Lead Bromide Quantum Dots. *Nano Lett.* **2018**, *18* (7), 4440−4446.
(53) Fu, M.; Tamarat, P.; Trebbia, J.-B.; Bodnarchuk, M. I.; Kovalenko, M. V.; Even, J.; Lounis, B. Unraveling Exciton−Phonon Coupling in Individual $FAPbI_3$ Nanocrystals Emitting Near-Infrared Single Photons. *Nat. Commun.* **2018**, *9* (1), 3318.
(54) Yarita, N.; Tahara, H.; Saruyama, M.; Kawawaki, T.; Sato, R.; Teranishi, T.; Kanemitsu, Y. Impact of Postsynthetic Surface Modification on Photoluminescence Intermittency in Formamidinium Lead Bromide Perovskite Nanocrystals. *J. Phys. Chem. Lett.* **2017**, *8* (24), 6041−6047.
(55) Almeida, G.; Goldoni, L.; Akkerman, Q.; Dang, Z.; Khan, A. H.; Marras, S.; Moreels, I.; Manna, L. Role of Acid−Base Equilibria in the Size, Shape, and Phase Control of Cesium Lead Bromide Nanocrystals. *ACS Nano* **2018**, *12* (2), 1704−1711.
(56) Ravi, V. K.; Santra, P. K.; Joshi, N.; Chugh, J.; Singh, S. K.; Rensmo, H.; Ghosh, P.; Nag, A. Origin of the Substitution Mechanism for the Binding of Organic Ligands on the Surface of $CsPbBr_3$ Perovskite Nanocubes. *J. Phys. Chem. Lett.* **2017**, *8* (20), 4988−4994.
(57) Akkerman, Q. A.; Park, S.; Radicchi, E.; Nunzi, F.; Mosconi, E.; De Angelis, F.; Brescia, R.; Rastogi, P.; Prato, M.; Manna, L. Nearly Monodisperse Insulator Cs_4PbX_6 (X = Cl, Br, I) Nanocrystals, Their Mixed Halide Compositions, and Their Transformation into $CsPbX_3$ Nanocrystals. *Nano Lett.* **2017**, *17* (3), 1924−1930.
(58) Balakrishnan, S. K.; Kamat, P. V. Ligand Assisted Transformation of Cubic $CsPbBr_3$ Nanocrystals into Two-Dimensional $CsPb_2Br_5$ Nanosheets. *Chem. Mater.* **2018**, *30* (1), 74−78.
(59) Liu, Z.; Bekenstein, Y.; Ye, X.; Nguyen, S. C.; Swabeck, J.; Zhang, D.; Lee, S. T.; Yang, P.; Ma, W.; Alivisatos, A. P. Ligand Mediated Transformation of Cesium Lead Bromide Perovskite Nanocrystals to Lead Depleted Cs_4PbBr_6 Nanocrystals. *J. Am. Chem. Soc.* **2017**, *139* (15), 5309−5312.
(60) Palazon, F.; Almeida, G.; Akkerman, Q. A.; De Trizio, L.; Dang, Z.; Prato, M.; Manna, L. Changing the Dimensionality of Cesium Lead Bromide Nanocrystals by Reversible Postsynthesis Transformations with Amines. *Chem. Mater.* **2017**, *29* (10), 4167−4171.
(61) Shamsi, j.; Dang, Z.; Ijaz, P.; Abdelhady, A. L.; Bertoni, G.; Moreels, I.; Manna, L. Colloidal CsX (X = Cl, Br, I) Nanocrystals and their Transformation to $CsPbX_3$ Nanocrystals by Cation Exchange. *Chem. Mater.* **2018**, *30* (1), 79−83.
(62) Udayabhaskararao, T.; Houben, L.; Cohen, H.; Menahem, M.; Pinkas, I.; Avram, L.; Wolf, T.; Teitelboim, A.; Leskes, M.; Yaffe, O.; et al. A Mechanistic Study of Phase Transformation in Perovskites Nanocrystals Driven by Ligand Passivation. *Chem. Mater.* **2018**, *30* (1), 84−93.
(63) Wu, L.; Hu, H.; Xu, Y.; Jiang, S.; Chen, M.; Zhong, Q.; Yang, D.; Liu, Q.; Zhao, Y.; Sun, B.; et al. From Nonluminescent Cs_4PbX_6 (X = Cl, Br, I) Nanocrystals to Highly Luminescent $CsPbX_3$ Nanocrystals: Water-Triggered Transformation through a CsX-Stripping Mechanism. *Nano Lett.* **2017**, *17* (9), 5799−5804.
(64) Zhai, W.; Lin, J.; Li, Q.; Zheng, K.; Huang, Y.; Yao, Y.; He, X.; Li, L.; Yu, C.; Liu, C.; et al. Solvothermal Synthesis of Ultrathin Cesium Lead Halide Perovskite Nanoplatelets with Tunable Lateral Sizes and Their Reversible Transformation into Cs_4PbBr_6 Nanocrystals. *Chem. Mater.* **2018**, *30* (11), 3714−3721.
(65) de Weerd, C.; Lin, J.; Gomez, L.; Fujiwara, Y.; Suenaga, K.; Gregorkiewicz, T. Hybridization of Single Nanocrystals of Cs_4PbBr_6 and $CsPbBr_3$. *J. Phys. Chem. C* **2017**, *121* (35), 19490−19496.
(66) Woo, J. Y.; Kim, Y.; Bae, J.; Kim, T. G.; Kim, J. W.; Lee, D. C.; Jeong, S. Highly Stable Cesium Lead Halide Perovskite Nanocrystals through in Situ Lead Halide Inorganic Passivation. *Chem. Mater.* **2017**, *29* (17), 7088−7092.
(67) Wang, C.; Chesman, A. S. R.; Jasieniak, J. J. Stabilizing the Cubic Perovskite Phase of $CsPbI_3$ Nanocrystals by Using an Alkyl Phosphinic Acid. *Chem. Commun.* **2017**, *53* (1), 232−235.
(68) Liu, F.; Zhang, Y.; Ding, C.; Kobayashi, S.; Izuishi, T.; Nakazawa, N.; Toyoda, T.; Ohta, T.; Hayase, S.; Minemoto, T.; et al. Highly Luminescent Phase-Stable $CsPbI_3$ Perovskite Quantum Dots Achieving Near 100% Absolute Photoluminescence Quantum Yield. *ACS Nano* **2017**, *11* (10), 10373−10383.
(69) Wu, L.; Zhong, Q.; Yang, D.; Chen, M.; Hu, H.; Pan, Q.; Liu, H.; Cao, M.; Xu, Y.; Sun, B.; et al. Improving the Stability and Size Tunability of Cesium Lead Halide Perovskite Nanocrystals Using Trioctylphosphine Oxide as the Capping Ligand. *Langmuir* **2017**, *33* (44), 12689−12696.
(70) Huang, S.; Wang, B.; Zhang, Q.; Li, Z.; Shan, A.; Li, L. Postsynthesis Potassium-Modification Method to Improve Stability of $CsPbBr_3$ Perovskite Nanocrystals. *Adv. Opt. Mater.* **2018**, *6* (6), 1701106.
(71) Wu, Y.; Wei, C.; Li, X.; Li, Y.; Qiu, S.; Shen, W.; Cai, B.; Sun, Z.; Yang, D.; Deng, Z.; et al. In-situ Passivation of $PbBr_6^{4-}$ Octahedrons towards Blue Luminescent $CsPbBr_3$ Nanoplatelets with Near 100% Absolute Quantum Yield. *ACS Energy Lett.* **2018**, *3* (9), 2030−2037.
(72) Lu, C.; Li, H.; Kolodziejski, K.; Dun, C.; Huang, W.; Carroll, D.; Geyer, S. M. Enhanced Stabilization of inorganic Cesium Lead Triiodide ($CsPbI_3$) Perovskite Quantum Dots with Tri-Octylphosphine. *Nano Res.* **2018**, *11* (2), 762−768.
(73) Guhrenz, C.; Benad, A.; Ziegler, C.; Haubold, D.; Gaponik, N.; Eychmüller, A. Solid-State Anion Exchange Reactions for Color Tuning of $CsPbX_3$ Perovskite Nanocrystals. *Chem. Mater.* **2016**, *28* (24), 9033−9040.
(74) Huang, H.; Chen, B.; Wang, Z.; Hung, T. F.; Susha, A. S.; Zhong, H.; Rogach, A. L. Water resistant $CsPbX_3$ Nanocrystals Coated with Polyhedral Oligomeric Silsesquioxane and their Use as Solid State Luminophores in All-Perovskite White Light-Emitting Devices. *Chem. Sci.* **2016**, *7* (9), 5699−5703.
(75) Meyns, M.; Peralvarez, M.; Heuer-Jungemann, A.; Hertog, W.; Ibanez, M.; Nafria, R.; Genc, A.; Arbiol, J.; Kovalenko, M. V.; Carreras, J.; et al. Polymer-Enhanced Stability of Inorganic Perovskite Nanocrystals and Their Application in Color Conversion LEDs. *ACS Appl. Mater. Interfaces* **2016**, *8* (30), 19579−19586.
(76) Quan, L. N.; Quintero-Bermudez, R.; Voznyy, O.; Walters, G.; Jain, A.; Fan, J. Z.; Zheng, X.; Yang, Z.; Sargent, E. H. Highly Emissive Green Perovskite Nanocrystals in a Solid State Crystalline Matrix. *Adv. Mater.* **2017**, *29* (21), 1605945−1605951.
(77) Raja, S. N.; Bekenstein, Y.; Koc, M. A.; Fischer, S.; Zhang, D.; Lin, L.; Ritchie, R. O.; Yang, P.; Alivisatos, A. P. Encapsulation of Perovskite Nanocrystals into Macroscale Polymer Matrices: Enhanced Stability and Polarization. *ACS Appl. Mater. Interfaces* **2016**, *8* (51), 35523−35533.
(78) Xu, L.; Chen, J.; Song, J.; Li, J.; Xue, J.; Dong, Y.; Cai, B.; Shan, Q.; Han, B.; Zeng, H. Double-Protected All-Inorganic Perovskite Nanocrystals by Crystalline Matrix and Silica for Triple-Modal Anti-Counterfeiting Codes. *ACS Appl. Mater. Interfaces* **2017**, *9* (31), 26556−26564.
(79) Li, Z.; Kong, L.; Huang, S.; Li, L. Highly Luminescent and Ultrastable $CsPbBr_3$ Perovskite Quantum Dots Incorporated into a Silica/Alumina Monolith. *Angew. Chem., Int. Ed.* **2017**, *56* (28), 8134−8138.
(80) González-Pedro, V.; Veldhuis, S. A.; Begum, R.; Bañuls, M. J.; Bruno, A.; Mathews, N.; Mhaisalkar, S.; Maquieira, Á. Recovery of Shallow Charge-Trapping Defects in $CsPbX_3$ Nanocrystals through

DOI: 10.1021/acsenergylett.8b01669
ACS Energy Lett. 2019, 4, 63−74

Specific Binding and Encapsulation with Amino-Functionalized Silanes. *ACS Energy Lett.* **2018**, *3*, 1409−1414.
(81) Zhang, X.; Wang, H.-C.; Tang, A.-C.; Lin, S.-Y.; Tong, H.-C.; Chen, C.-Y.; Lee, Y.-C.; Tsai, T.-L.; Liu, R.-S. Robust and Stable Narrow-Band Green Emitter: An Option for Advanced Wide-Color-Gamut Backlight Display. *Chem. Mater.* **2016**, *28* (23), 8493−8497.
(82) Bertolotti, F.; Protesescu, L.; Kovalenko, M. V.; Yakunin, S.; Cervellino, A.; Billinge, S. J. L.; Terban, M. W.; Pedersen, J. S.; Masciocchi, N.; Guagliardi, A. Coherent Nanotwins and Dynamic Disorder in Cesium Lead Halide Perovskite Nanocrystals. *ACS Nano* **2017**, *11* (4), 3819−3831.
(83) Swarnkar, A.; Chulliyil, R.; Ravi, V. K.; Irfanullah, M.; Chowdhury, A.; Nag, A. Colloidal $CsPbBr_3$ Perovskite Nanocrystals: Luminescence beyond Traditional Quantum Dots. *Angew. Chem., Int. Ed.* **2015**, *54* (51), 15424−15428.
(84) Nedelcu, G.; Protesescu, L.; Yakunin, S.; Bodnarchuk, M. I.; Grotevent, M. J.; Kovalenko, M. V. Fast Anion-Exchange in Highly Luminescent Nanocrystals of Cesium Lead Halide Perovskites ($CsPbX_3$, X = Cl, Br, I). *Nano Lett.* **2015**, *15* (8), 5635−5640.
(85) Beck, J. S.; Vartuli, J. C.; Roth, W. J.; Leonowicz, M. E.; Kresge, C. T.; Schmitt, K. D.; Chu, C. T. W.; Olson, D. H.; Sheppard, E. W.; McCullen, S. B.; et al. A New Family of Mesoporous Molecular Sieves Prepared with Liquid Crystal Templates. *J. Am. Chem. Soc.* **1992**, *114* (27), 10834−10843.
(86) Kresge, C. T.; Leonowicz, M. E.; Roth, W. J.; Vartuli, J. C.; Beck, J. S. Ordered Mesoporous Molecular Sieves Synthesized by a Liquid-Crystal Template Mechanism. *Nature* **1992**, *359*, 710−712.
(87) Osman, M. A.; Ernst, M.; Meier, B. H.; Suter, U. W. Structure and Molecular Dynamics of Alkane Monolayers Self-Assembled on Mica Platelets. *J. Phys. Chem. B* **2002**, *106* (3), 653−662.
(88) Xie, W.; Gao, Z.; Pan, W.-P.; Hunter, D.; Singh, A.; Vaia, R. Thermal Degradation Chemistry of Alkyl Quaternary Ammonium Montmorillonite. *Chem. Mater.* **2001**, *13* (9), 2979−2990.
(89) Heinz, H.; Vaia, R. A.; Farmer, B. L. Relation between Packing Density and Thermal Transitions of Alkyl Chains on Layered Silicate and Metal Surfaces. *Langmuir* **2008**, *24* (8), 3727−3733.
(90) Heinz, H.; Suter, U. W. Surface Structure of Organoclays. *Angew. Chem., Int. Ed.* **2004**, *43* (17), 2239−2243.
(91) Kovalenko, M. V.; Bodnarchuk, M. I.; Talapin, D. V. Nanocrystal Superlattices with Thermally Degradable Hybrid Inorganic−Organic Capping Ligands. *J. Am. Chem. Soc.* **2010**, *132* (43), 15124−15126.
(92) Zhang, D.; Yang, Y.; Bekenstein, Y.; Yu, Y.; Gibson, N. A.; Wong, A. B.; Eaton, S. W.; Kornienko, N.; Kong, Q.; Lai, M.; et al. Synthesis of Composition Tunable and Highly Luminescent Cesium Lead Halide Nanowires through Anion-Exchange Reactions. *J. Am. Chem. Soc.* **2016**, *138* (23), 7236−7239.
(93) Wang, H.; Sui, N.; Bai, X.; Zhang, Y.; Rice, Q.; Seo, F. J.; Zhang, Q.; Colvin, V. L.; Yu, W. W. Emission Recovery and Stability Enhancement of Inorganic Perovskite Quantum Dots. *J. Phys. Chem. Lett.* **2018**, *9* (15), 4166−4173.
(94) deQuilettes, D. W.; Koch, S.; Burke, S.; Paranji, R. K.; Shropshire, A. J.; Ziffer, M. E.; Ginger, D. S. Photoluminescence Lifetimes Exceeding 8 μs and Quantum Yields Exceeding 30% in Hybrid Perovskite Thin Films by Ligand Passivation. *ACS Energy Lett.* **2016**, *1* (2), 438−444.
(95) Abdi-Jalebi, M.; Andaji-Garmaroudi, Z.; Cacovich, S.; Stavrakas, C.; Philippe, B.; Richter, J. M.; Alsari, M.; Booker, E. P.; Hutter, E. M.; Pearson, A. J.; et al. Maximizing and Stabilizing Luminescence from Halide Perovskites with Potassium Passivation. *Nature* **2018**, *555*, 497−501.

DOI: 10.1021/acsenergylett.8b01669
ACS Energy Lett. 2019, 4, 63−74